RSC Advances

PAPER

View Article Online
View Journal | View Issue

Iron–chromium oxide nanoparticles self-assembling into smectic mesophases†

Cite this: *RSC Adv.*, 2014, **4**, 6293

M. Iacob,[ab] M. Cazacu,*[a] C. Racles,[a] M. Ignat,[a] V. Cozan,[a] L. Sacarescu,[a] D. Timpu,[a] M. Kajňaková,[c] M. Botko,[c] A. Feher[c] and C. Turta[ab]

Received 26th November 2013
Accepted 18th December 2013

DOI: 10.1039/c3ra47072e

www.rsc.org/advances

Organic-coated iron–chromium oxide (chromite) nanoparticles have been prepared by using the thermal decomposition procedure. For this purpose, the substrate – bimetallic acetate – was treated with oleic acid and dodecylamine as co-ligands in trichloroacetic acid solvent at high temperature (320 °C). The main characteristics and behaviors of the obtained nanoparticles were investigated by combined techniques. The size of the obtained nanoparticles was around 11 nm, as estimated by TEM, WAXD and SAXS, which were in good agreement. The bimetallic nature of the nanoparticles was emphasized by X-ray energy dispersive spectrometry (EDX) and their structure was confirmed by WAXD. The Fourier transform infrared (FTIR) spectrum revealed the bands characteristic to metal oxides as well as to the organic components and confirmed the replacement of the acetate with long chain ligands. The co-existence of the organic coatings and metallic core induced a special behavior that was studied by thermogravimetric analysis, differential scanning calorimetry and polarized optical microscopy. The coated bimetallic nanoparticles proved to be thermostable up to 252 °C and thermotropic showing a highly organized crystalline smectic mesophase (3D plastic mesophase). The organic part alone, in the absence of the inorganic component, did not develop this self-assembly. The results of the magnetic measurements suggest superparamagnetic behavior of the iron–chromium oxide nanoparticles and a weak ferromagnetic behavior.

Introductions

The research in the field of nanoparticles presents both theoretical and practical interest. Due to their unique properties, nanoparticles are of interest in medicine, biology, optics and electro-optics, catalysis, environmental protection and many others.[1] Mixed metal oxide nanoparticles (also called hetero-metal oxide nanoparticles) can play an important role in many areas of chemistry and physics due to the unique electronic and magnetic properties obtained by combining two metals in an oxide matrix. The most common application for metal oxide nanoparticles has been in the area of catalysis, where they have been used either as catalyst or catalyst support. In addition, since these materials showed ferro- or pyroelectric properties, they found recently interesting applications in the electronic industry as passive or active components in specific devices.[2]

Chromium–iron oxide (chromite), in particular, has been explored in the last two decades due to their improved catalytic activity in certain reactions as compared to the corresponding Fe- or Cr-catalysts alone. The unique performance of Cr–Fe catalysts was assigned to the role of chromium in stabilizing the iron oxide against sintering, slow down the ageing effect and reducing the surface area.[3,4] Besides acting as a textural promoter, chromium may act as a structural promoter which is also important in enhancing the catalytic activity and stability.[5]

Different strategies have been approached to prepare mixed iron–chromium oxide.[3,6–8] In general, the used procedures started from salt mixture of the two metals (*e.g.*, chlorides,[6] nitrates[7] or chloride–nitrate[8]) processed by sonochemical,[3,8] or hydrothermal methods,[6] solid or solution thermal decomposition,[7] in the presence or not of some organic component (a mixture of polyethyleneglycol and urea,[8] citric acid as a fuel,[7] *etc.*). Such methods are generally used to obtain iron–chromium oxide but also other metallic oxides.[9–11]

Supramolecular surfactant-controlled method was also applied for the synthesis of mesostructured iron oxides by using neutral or charged template molecules. Thus, different surfactants were used as a template: *n*-alkyl sulphate,[12] polyisobutylene bissuccinimide,[13] a microbial-derived surfactant

[a]"Petru Poni" Institute of Macromolecular Chemistry Iasi, Aleea Gr. Ghica Voda 41 A, 700487, Romania. E-mail: mcazacu@icmpp.ro

[b]Institute of Chemistry of ASM, Academiei str. 3, Chisinau 2028, Republic of Moldova. E-mail: turtalcba@gmail.com

[c]Center of Low Temperature Physics, Faculty of Science, P. J. Šafárik University, Park Angelinum 9, 04154 Košice, Slovakia

† Electronic supplementary information (ESI) available: FTIR and EDX spectra for NPs sample, FTIR spectrum for Sfs sample, FTIR and EDX spectra of μ_3-oxo heterotrinuclear {$FeCr_2O$} acetate, the XRD peak assignment (*d* spacing values). See DOI: 10.1039/c3ra47072e

(MDS),[14] polyacrylic acid sodium salt (PAA),[15] hexadecyltrimethylammonium bromide (HDTMA) or cetyltrimethylammonium bromide (CTAB).[16] It is well known that inorganic anions like chloride, phosphate or sulfate have also a strong influence on particle size and shape.[15] For biology and medicine applications, for example, it is almost always necessary to incorporate the nanoparticles into more complex structure, often through the use of a suitable organic coating, which not only imparts stability against aggregation but also provides solubility, modularity, optical and self-organization properties.[1] If such a structure is of liquid crystalline kind, then it would be possible to manipulate the nanoparticles in the 2D or 3D space, to gain higher processability and self-healing properties.[1] Rods or plate like particles could form additional liquid crystalline phases with nematic or smectic order. The spontaneous formation of such phases is nowadays often called self-assembly or self-organization.[17] It has been shown experimentally that the spontaneous onset of LC ordering could be a way to obtain very well aligned NPs.[18]

Unlike these studies, in this work we used as oxide precursor a preformed bimetallic cluster, μ_3-oxo heterotrinuclear $\{FeCr_2O\}$ acetate with 1 : 2 iron : chromium molar ratio, that to permit the obtaining of nanoparticles with well defined, pre-established metal ratio. A long chain organic ligand–surfactant mixture (oleic acid and dodecylamine) was added to facilitate the obtaining of nanoparticles. The product obtained in an one-step approach consisting in the thermal decomposition of the mixture shown above was characterized by spectral (FTIR, EDX) analysis, TEM, XRD, TGA, DSC and POM. The magnetic properties of the resulted materials were also investigated.

Results and discussion

Iron–chromium oxide (chromite) nanoparticles, NPs, have been prepared by a one-step procedure consisting in the thermal decomposition of μ_3-oxo heterotrinuclear $\{FeCr_2O\}$ acetate (ICC) as oxide precursor admixed with oleic acid (OA) and high excess of dodecylamine (DA) as surfactants (1 : 0.3 : 17 molar ratio) in solvent trichloroacetic acid (TCAA) (Scheme 1). The organic mixture without metallic precursor was processed in the same conditions obtaining sample Sfs, which was used as reference to evaluate the influence of the metallic core on the behavior of the organic coating.

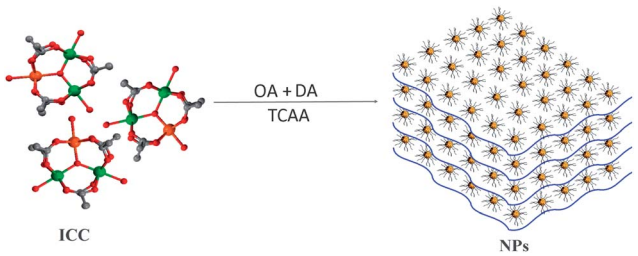

Scheme 1 A graphical representation of the process of forming and self-assembling nanoparticles (OA – oleic acid, TCAA – trichloroacetic acid, DA – dodecylamine, ICC – iron–chromium carboxy-cluster).

According to literature data, at elevated temperature (above 300 °C), multiple processes occur: progressive ligand substitution (acetic acid is replaced by oleic acid), decomposition of metal aliphatic carboxylates with formation of oxide nanoparticles[19,20] and stabilization of the nanoparticles by dodecylamine and oleic acid. In addition, in the present case, due to atypical reagent ratio, we observed self-assembly of the organic coated nanoparticles, as will be discussed hereafter.

In the FTIR spectrum of NPs (Fig. 1), the bands characteristic to metal oxides were present in the range 600–400 cm^{-1}. The band at 540 cm^{-1} is assigned to the Cr–O lattice vibration, while a wider band centered at 621 cm^{-1} could be assigned to Fe–O lattice vibrations as the literature indicates.[21]

Many other bands characteristic for organic compounds used in synthesis are also present. Two pairs of bands at 2956, 2870 and 2919, 2850 cm^{-1} assigned to asymmetrical and symmetrical stretching vibrations, $\nu_{as,s}$(C–H) from CH_3 and CH_2 groups, respectively[22] are due to dodecylamine and oleic acid. Another pair of bands at 1550 and 1434 cm^{-1} are assigned to stretching vibrations $\nu_{as,s}(COO^-)$ from oleate groups, which were demonstrated to exist at the surface of the oxide NPs.[23]

From Fig. 1 (inset), it can be observed that there is a significant shift of the bands (from 1604 and 1454 cm^{-1}, respectively), compared with the starting acetate. This shows that the acetate ligand was substituted by oleic acid. In addition, there is no carboxylic acid band present in the spectrum. On the other hand, it was demonstrated[23] that during the thermal treatment, the oleic acid suffers chemical modifications that lead to loose of unsaturation. In FT-IR spectrum, such a modification is indeed observed in this case, too, by disappearance of the vinyl band at 3005 cm^{-1}. The bands at 3314, 3415 cm^{-1} and 1641 cm^{-1} indicate the presence of dodecylamine on the surface of oxide nanoparticles.

The FT-IR spectrum of the organic phase processed in the same way (Fig. 1) confirms the existence of a mixture of ligand

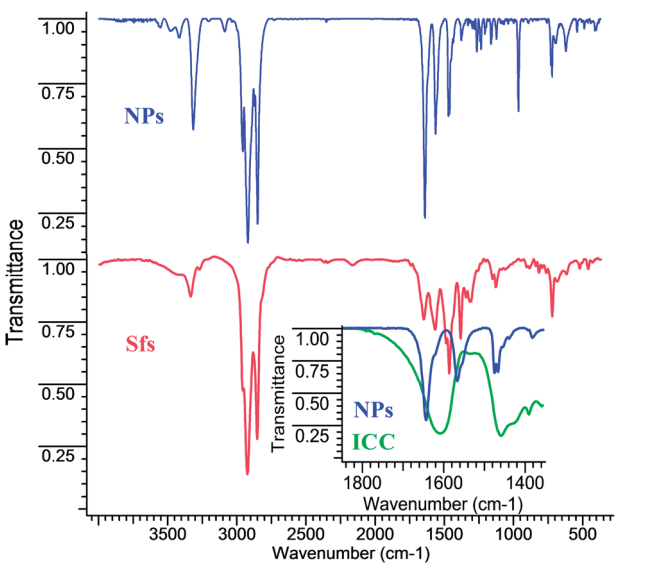

Fig. 1 FTIR spectra for NPs, Sfs, and ICC (iron–chromium carboxy-cluster).

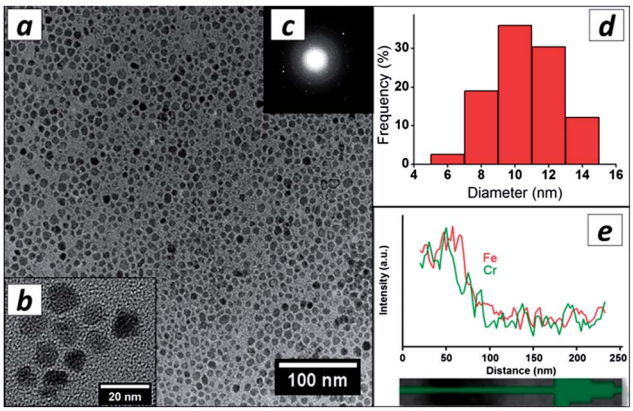

Fig. 2 TEM images of nanoparticles (a and b), small area electron diffraction pattern (c), size distribution nanoparticles histogram (d) and EDX line scan of the nanoparticles (e).

components. The bands characteristic to dodecylamine (3322, 3429, 1649 cm^{-1}) are well represented, while the carboxylic acid bands (1706 cm^{-1} free and 1741cm^{-1} H-bonded) are very weak (shoulders), which in fact is normal considering the reagents ratio.

TEM images taken on nanoparticles dispersion sprayed on carbon coated copper grid are shown in Fig. 2a and b. It can be seen that the particles are varied in shape and size. The electron diffraction pattern (Fig. 2c) is a proof for the crystallinity of the sample. Images were processed with ImageJ 3.0 to obtain the derived histogram (Fig. 2d) from 351 particles. According to this histogram, ~85% of the particles have a size ranging between 6 and 14 nm, with an average size of 10.6 nm. The EDX scanned lines of 250 nm samples (Fig. 2e) demonstrate the presence of iron and chromium in the nanoparticles. High intensities of the signals assigned to the metals were registered on the TEM grid covered with nanoparticles while the intensity of the signal is close to zero on the surface of the grid not covered with nanoparticles. By this technique, the EDX quantitative analysis is not precise, due to very low amount (thickness) of the sample. This is why we used EDX analysis from SEM for quantitative assessment (Fig. S1†). The presence of iron and chromium is clearly revealed and, in addition, the atomic ratio between the two metals was found 1.8 (Cr/Fe), which is in agreement with the ratio in the proposed structure: $FeCr_2O_4$. The EDX also showed the presence of N from dodecylamine, which confirms the hypothesis of amine covering the nanoparticles. In addition, no chlorine was detected by EDX, thus confirming the complete removal of trichloroacetic acid during reaction and purification steps.

Wide Angle X-ray powder diffraction was measured on samples NPs and Sfs at room temperature (Fig. 3). For sample NPs, one can observe sharp diffraction peaks both in the medium angle region (1.3–30° 2Θ) and the wide angle region (30–70° 2Θ). These two regions were treated separately. First, the peak assignment (d spacing values) in the wide angle region was made according to literature data and corresponds to well-established structure of iron–chromium oxide (as described in

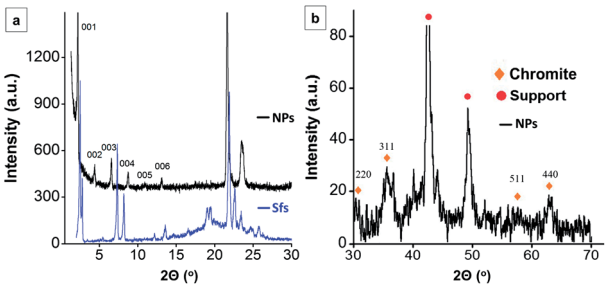

Fig. 3 X-ray powder diffraction pattern of nanoparticles, NPs (black lines), and Sfs (blue line) samples at room temperature in the medium angle region (1.3–30° 2Θ) (a) and pattern of NPs in the wide angle region (30–70° 2Θ) (b).

ICCD 34-140) (Table S1†). Appling Scherrer formula,[24] the crystallite size was calculated as being 11.3 nm. This value is in good agreement with the average size measured on TEM images.

The second aspect revealed by the powder X-ray diffraction spectrum is the presence of several peaks in 1.3–30° 2Θ region. This fact indicates a self-assembling of the nanoparticles, forming ordered layered structures. In Table 1, the 2Θ values, Bragg distances d, the scattering vectors, $Q = 2\pi/d$ (ref. 25) and the successive ratios of Q_i/Q_1 (where i = 1–6), are presented. As can be observed, the six small – medium angle reflections are in the ratio 1 : 2 : 3 : 4 : 5 : 6, which indicates a highly ordered layered structure. This kind of ordering was reported by other authors[26] and assigned to crystalline smectic phase.

For sample Sfs, it can be observed that the spectrum (Fig. 3a) shows different positions of the diffraction peaks when compared with the spectrum of NPs (Fig. 3a). The mixture of organic components (oleic acid and dodecyl amine) presented a sharp diffraction peak at 2.48° (2θ), corresponding to a Bragg distance of 35.6 Å. Considering the fact that the two organic components could interact (by hydrogen bonds or chemical-amide-bonds), a Hyperchem simulation of the geometry of an amide chemical model (Fig. S2†) gave a molecular length in totally extended form of 36.8 Å. Thus it is reasonable to presume that the molecular associates formed by the two components exhibit a smectic mesomorphism with a layer spacing of around 36 Å. This is *per se* an interesting result, and further investigations are needed to observe the influence of different factors, like reagents ratio, presence of trichloroacetic acid, temperature *etc.*, on the self-assembling in this system. For now, we only

Table 1 X-ray powder diffraction data for nanoparticles sample at room temperature

Number of peak	2θ (°)	Bragg distance, d (Å)	Wave vector, Q (Å^{-1})	Wave vectors ratio, Q_i/Q_1, (i = 1 ÷ 6)
1	2.18	40.5	0.155	1.00
2	4.39	20.2	0.313	2.01
3	6.57	13.5	0.468	3.01
4	8.72	10.1	0.620	4.00
5	10.89	8.1	0.774	4.99
6	13.13	6.7	0.933	6.01

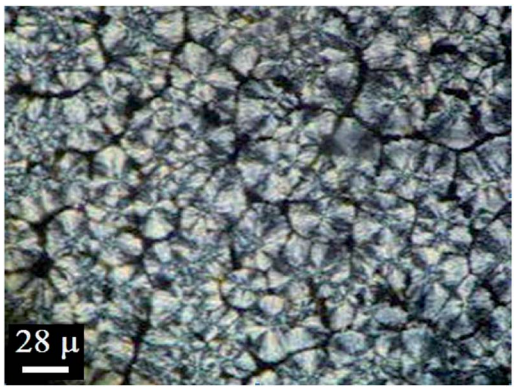

Fig. 4 Optical polarized light image of nanoparticles sample at 50 °C under cooling.

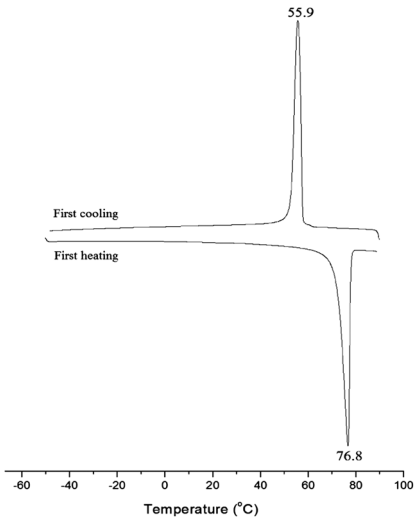

Fig. 5 DSC thermogram of nanoparticles (NPs) at a heating/cooling rate of 10 °C min^{-1} under nitrogen.

wanted to compare the observations on NPs sample with a "blind" one, obtained in the same way, but without metallic precursor. The sharp and strong diffraction peak at 21.6 in NPs and 21.9 in Sf, with a corresponding *d* value of 4.1 (4.05) Å might be assigned to transversal dimension of the surfactant molecules.

By comparing the two XRD spectra, it is obvious that the smectic crystal ordering is characteristic for the nanocomposite material (NPs) and this organization is completely different from the mixture of organics processed in the same conditions. Thus, it is reasonable to conclude that the metallic core is responsible for inducing the high order in this material. A schematic of the NPs self-assembling is shown in Scheme 1.

The influence of metallic nanoparticles on liquid crystalline compounds was reported in the literature. For example, the presence of metal nanoparticles (Au nanoparticles) was found to influence the stability of liquid crystals phases[27] and/or the mesophase range.[28] Other studies reported pronounced enhancement of birefringence and dielectric anisotropy of liquid crystals in presence of ferroelectric nanoparticles.[29]

The nanoparticles sample, NPs, was further investigated under thermal exposure by using polarizing light microscopy. At heating, the soft birefringent material melted into an isotropic fluid. At cooling, a birefringent spherulitic texture occurred around 53 °C (Fig. 4). Applying of a shearing stress on the upper lamella revealed that the texture is not fluid but like a soft solid. This observation confirms the X-ray diffraction data, pointing towards smectic crystals. It is known that liquid crystals are fluid materials, while higher ordered smectic crystals are an intermediate class of materials between common crystals and liquid crystals.[25,30]

Calorimetric measurements (DSC) were performed to confirm the behavior of the sample as observed by the polarized light optical microscopy. As can be observed in Fig. 5, at heating, the crystalline material melted at 76.8 °C to an isotropic liquid. When cooling, this isotropic liquid crystallizes at 55.9 °C in agreement with the microscopy observations. It is important to observe that these calorimetric data demonstrate that our sample behaves like a unitary homogeneous compound, as expected from the nanoparticle synthesis approach.

The organic part alone, in the absence of the inorganic component, presented a completely different thermal behavior in DSC: multiple endothermal peaks (within 40–120 °C range) in the first heating, two exothermic peaks on cooling and two endotherms in the second heating scan, at 16.4 and 32.4 °C (Fig. S3†). This confirms a liquid crystalline phase, which is however different from the NPs self-assembling. The surfactants mixture was also analyzed by optical polarized microscopy and exhibited a mosaic-like texture (Fig. S4†). This texture is frequently encountered in the case of smectic phases and is not specific for a crystallization process. The image is different from that of nanoparticles which showed a spherulitic texture (Fig. 4).

The chromite nanoparticles were further characterized by small angle X-ray scattering (SAXS). This study (Fig. 6) confirmed the lamellar structure of the organic fraction coating oxide nanoparticles. The intensity of the scattering pattern (*I*, a.u.) was plotted *versus* the scattering vector modulus *q* (nm^{-1}), showing the Bragg peak intensities for specific values of the scattering vector *q* in SAXS curves. The lamella repeat distance, *D*, was calculated as an average value from the first and second order of diffraction according to $D = 2\pi/q_1$ for the first order of

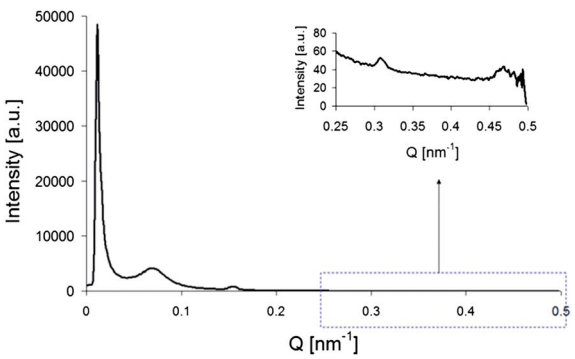

Fig. 6 Small angle X-ray scattering (SAXS) patterns for NPs sample.

diffraction peak and $D = 4\pi/q_2$ for the second order of diffraction peak. This distance was found to be 41 Å. The size of the nanoparticles (R_g) has been calculated from the Guinier plot. The estimated R_g was found to be 11.7 nm, assuming globular particles. Thus, the SAXS results are in good agreement with WAXD, both concerning the inter-lamellar distance (see Table 1) and nanoparicles size.

The thermal stability of the organic-coated nanoparticles was investigated by thermogravimetrical analysis (Fig. 7) and the results were compared with those of the model organic phase Sfs, as well as with those for starting cluster. In the NPs sample, on the TG and DTG lines (Fig. 7a) it can be observed that up to 252 °C there aren't any processes with mass loss. In the DTA curve, the endothermal peak detected at T_{max} = 76.92 °C is in agreement with the DSC scan (Fig. 5) and can be assigned to the melting process. The main decomposition process takes place in the limits of temperature ~252–442 °C with T_{max} ~ 387 °C (DTG) and it could be assigned to evaporation/decomposition of the surfactants that form the protective shell of the nanoparticles. The peak value on DTG curve is close to the boiling point of oleic acid (360 °C). The weight loss during the thermal evaporation/decomposition is more than 85 wt% of the initial mass; based on this, it might be estimated that the weight ratio between the surfactant shell and the iron–chromium oxide is quite large, ~4 : 1. Based on the found nitrogen content (2.5 wt%), it could be estimated that about 33 wt% from the hybrid nanomaterial consist in dodecylamine.

In Fig. 7b it can be noticed that the organic phase Sfs has a lower thermal stability, losing mass in several steps starting at about 83 °C. This behavior can be attributed to the higher volatility of organic ingredients that are not involved in the coordination to metal ions as in nanoparticles. However, the main decomposition process occurred at around 400 °C, similar to NPs. Less thermally stable as compared with derived organic covered NPs proved to be also the starting iron–chromium acetate (Fig. S5†). The thermal decomposition for this occurs mainly in two steps: first takes places in the range 62.93–237.97 °C including a few other processes summarizing a mass loss of 28.86 wt%, while the second one ranges between 303.71 and 430.61 °C with a maximum at 370.37 °C, the mass loss in this step being 34.07 wt%. The residual mass in this case, 35.21 wt%, is higher as compared with that remained in the case of the NPs, this revealing a lower content in organic component of the aceto-cluster.

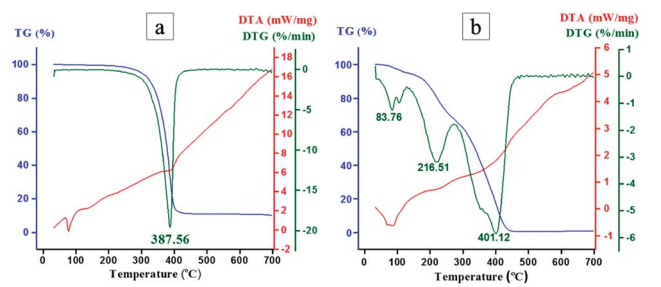

Fig. 7 TG, DTG and DTA curves recorded in nitrogen atmosphere for nanoparticles (NPs) (a) and Sfs (b).

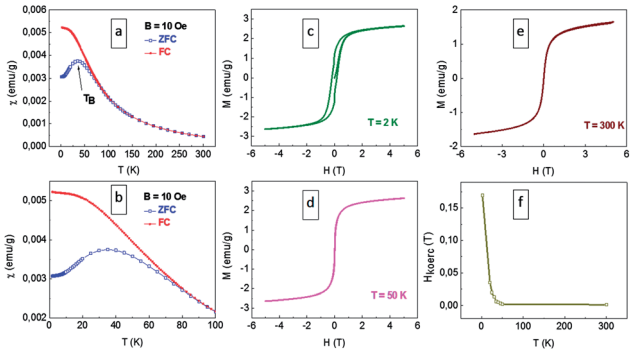

Fig. 8 Magnetic measurements of studied compound: (a) the mass-magnetic susceptibility of the sample, measured in zero-field-cooling and field-cooling regimes, in the magnetic field of 1 mT (10 Oe); (b) zoom of the graph (a) around the blocking temperature (TB) point; (c) the hysteresis loops of the sample at 2 K; (d) the hysteresis loops of the sample at 50 K; (e) the hysteresis loops of the sample at 300 K; (f) the temperature dependence of coercive field.

The dc-susceptibility was measured in applied magnetic field of 10 Oe (1 mT) in the temperature range 2–300 K in ZFC and FC regimes (Fig. 8a and b).

The temperature dependence of the susceptibility of sample studied in ZFC and FC regimes, exhibits the main features of superparamagnetic systems: the ZFC curves are maximum-rounded at the blocking temperature T_B ~ 38 K (in magnetic field 1 mT), defined as the temperature of a blocking process of the small particles. A paramagnetic-like behavior is observed above T_B.[31,32] The magnetization hysteresis loop at 2 K (Fig. 8c) indicates ferromagnetic interactions in the material with the coercive field 18.0 mT due to blocking the magnetic moments of nanoparticles by external magnetic field. Although sharp decrease of the coercive field H_c was observed in the vicinity of T_B (Fig. 8f), the weak hysteresis (~2 mT) still exists above T_B (Fig. 8d and e). Considering the shapes of ZFC and FC curves obtained from measurements of dc-susceptibility, which clearly indicate the superparamagnetic nature of the material, the existence of hysteresis above T_B could be the result of presence of small magnetic field frozen in the superconducting magnet. Further study of the magnetic properties of this material, including the measurements and analysis of ac-susceptibility, is beyond the scope of this article and will be discussed separately.

Experimental section

Materials

The heteronuclear iron–chromium acetate ($[FeCr_2O(CH_3COO)_6(H_2O)_3]\cdot NO_3$), {$FeCr_2O$}, was prepared following an already reported procedure[33] by using $Fe(NO_3)_3\cdot 9H_2O$ (Sigma Aldrich), $Cr(NO_3)_3\cdot 9H_2O$ (Sigma Aldrich), in 1 : 2 molar ratio and calcium acetate monohydrate, ($Ca(CH_3COO)_2\cdot H_2O$) (Sigma Aldrich), glacial acetic acid (Chemical Company), and distilled water. The chemical structure of the compound was verified by FTIR (Fig. S6†) and EDX (Fig. S7†). IR (KBr): ν = 411(m), 621(s), 642(m), 673(s), 835(w), 957(w), 1038(m), 1049(m), 1352(s), 1385(s), 1454(vs), 1605(vs), 3466 cm^{-1} (m).

Trichloroacetic acid, CCl_3COOH, (Fluka), dodecylamine, $CH_3(CH_2)_{11}NH_2$, (Fluka), oleic acid, $CH_3(CH_2)_7CH{=}CH(CH_2)_7COOH$, (Sigma Aldrich), hexane and ethanol (Chemical Company) were used as received.

Equipment

An Energy Dispersive X-Ray system (EDX) available on Environmental Scanning Electron Microscope (ESEM) type Quanta 200 was used for qualitative analysis and elemental mapping. The infrared spectra were registered on a Bruker Vertex 70 FT-IR instrument, in transmission mode, in the 300–4000 cm^{-1} range (resolution 2 cm^{-1}, 32 scans), at ambient temperature. Transmission Electron Microscopy (TEM) investigation was made with Hitachi High-Tech HT7700 Transmission Electron Microscope operated at 100 kV accelerating voltage in high contrast mode. The samples were prepared on carbon coated copper grids of 200 mesh size. Microdrops of the nanoparticles dispersed in hexane (0.1%) were placed on the grids, and then solvent was removed in vacuum. Wide Angle X-rays Diffraction (WAXD) was performed on a Bruker-AXS D8 ADVANCE diffractometer, with Bragg Brentano parafocusing goniometer. Scans were recorded in step mode using Ni-filtered Cu Kα radiation ($\lambda = 0.1541$ nm). The working conditions were 40 kV and 30 mA tube power. The Bruker computer softwares Eva 11 and Topaz 3.1 were used to plot and process the data. Small Angle X-ray Scattering (SAXS) was used to characterize the nanometric structure of the powdered sample phase. Data was collected at the Bruker-Nanostar U apparatus equipped with a 3-pinhole collimation system that provides a precisely parallel X-ray beam with high intensity and virtually no background so that fast measuring times and extremely high resolution can be achieved. The scattering intensity was measured as a function of scattering vector, q, being defined as $q = (4\pi/\lambda)\sin\theta$, where 2θ is the scattering angle and λ is the X-ray wavelength (1.54 Å). The space group has been determined using SGI (space group indexing) software. Thermogravimetric analyses (TGA) were performed on a Mettler Toledo TGA-SDTA851e type derivatograph (thermogravimetric analyzer) under nitrogen flow (20 ml min^{-1}), within 25–1000 °C range, at 10 °C min^{-1} heating rate for samples of 2–5 mg each. Alumina crucibles (70 µl) were used as sample holders. Every experiment was repeated three times and showed a good reproducibility. The data were processed using the STAR software Mettler Toledo. DSC measurements were conducted with a DSC 200 F3 Maia (Netzsch, Germany). About 9 mg of sample was heated in pressed and punched aluminium crucibles at a heating rate of 10 °C min^{-1}. Nitrogen was used as inert atmosphere at a flow rate of 100 ml min^{-1}. Magnetic measurements were performed in powders conditioned in inert gelatine capsules with a Quantum Design SQUID (superconducting quantum interference device) magnetometer (MPMS). The background correction of the signal resulting from the gelcap and a sample holder was defined from independent run with empty gelcap and subtracted from the total signal. The dc-magnetizations were measured in applied magnetic field of 10 Oe (1 mT) in the temperature range 2–300 K in zero-field-cooling (ZFC) and field-cooling (FC) regimes. The magnetization hysteresis loop was measured at 2 K and 300 K up to 5 T. To determine the coercivity field at 2 K and 300 K, the sample was cooled in zero applied magnetic field from room temperature down to the measuring temperature. Additional measurements of field dependence of magnetization have been done at 20 K, 25 K, 30 K, 35 K, 40 K, 45 K and 50 K.

Preparation of organic-coated iron chromite nanoparticles (NPs)

The mixture consisting of mixed iron–chromium acetate ($[FeCr_2O(CH3COO)_6(H_2O)_3]\cdot NO_3$) (0.8 g, 1.27 mmol), dodecylamine (4 g, 21.58 mmol), trichloroacetic acid (5 g, 30 mmol) and oleic acid (0.12 ml, 0.38 mmol) was stepwise heated until 320 °C in a three-necked flask equipped with condenser, thermometer and heating mantle and maintained for 1 h at this temperature. Then, the mixture was gradually cooled at room temperature, diluted with 75 ml hexane and filtered. The filtrate was centrifuged 15 min at 6000 rpm. The separated solid was washed three times with ethanol and dried to yield a brown-black powder. IR (KBr): ν = 540(vw), 621(w), 720(w), 729(w), 962(m), 1123(vw), 1163(w), 1206(vw), 1234(w), 1241(w), 1265(w), 1377(vw), 1435(w), 1450(w), 1463(m), 1471(m), 1563(m), 1641(s), 2850(vs), 2872(m), 2919(vs), 2956(m), 3315(m), 3415 cm^{-1} (vw) (Fig. S1†). Found nitrogen content value, N_2: 2.5 wt%.

Preparation of blank sample – without metal oxide core (Sfs)

The mixture consisting in dodecylamine (4 g, 21.58 mmol), trichloroacetic acid (5 g, 30 mmol) and oleic acid (0.12 ml, 0.38 mmol) was stepwise heated until 320 °C in a three-necked flask equipped with condenser, thermometer and heating mantle and maintained for 1 h at this temperature. Then, the mixture was gradually cooled at room temperature, diluted with 75 ml hexane and filtered. A yellow solid remained after filtrate evaporation, which was characterized as such. IR (KBr): ν = 721(w), 1126(w), 1153(w), 1315(w), 1344(w), 1383(m), 1466(m), 1489(m), 1568(m), 1649(w), 2853(s), 2924(vs), 2955(s), 3333 cm^{-1} (w).

Conclusions

A procedure was developed for obtaining magnetic nanoparticles of mixed metal (Fe–Cr) oxide using the thermal decomposition process of the μ_3-oxo heterotrinuclear $\{FeCr_2O\}$ acetate in the presence of oleic acid and dodecylamine as surfactants and trichloacetic acid as solvent. The main characteristics and behaviors of the obtained nanoparticles were investigated by combined techniques. The average size of the obtained nanoparticles is around 11 nm as determined by TEM, WAXD and SAXS and the atomic ratio between Fe and Cr was 1 : 1.8, based on EDX. The nanoparticles exhibit superparamagnetism with blocking temperature TB ~38 K. The magnetization hysteresis loop at 2 K indicates ferromagnetic interactions in the material with the coercive field, H_c = 18.0 mT. Based on TGA data, the molar ratio between the surfactant shell on the particles surface and mixed oxide was estimated as being ~4 : 1. WAXD and SAXS studies emphasized the lamellar structure of the organic coated oxide nanoparticles.

Highly ordered smectic crystal phase was detected based on XRD data and was confirmed by POM observations. The main structural, thermal and thermotropic data were compared with similar investigations conducted on a model sample, prepared in the same conditions without the metal precursor. We concluded that the high order is induced by the presence of metal oxide nanoparticles.

Acknowledgements

Authors would like to thank Dr Zeleňáková for helpful discussion concerning interpretation of magnetic measurements. This research was financially supported by European Regional Development Fund, Sectoral Operational Programme "Increase of Economic Competitiveness", Priority Axis 2 (SOP IEC-A2-O2.1.2-2009-2, ID 570, COD SMIS-CSNR: 12473, Contract 129/2010-POLISILMET) and by the Slovak Research and Development Agency under the contract no. APVV-0132-11 and the Slovak Grant AgencyVEGA 1/0145/13.

Notes and references

1 L. Nealon, R. Greget, C. Dominguez, Z. T. Nagy, D. Guillon, J.-L. Gallani and B. Donnio, *Beilstein J. Org. Chem.*, 2012, **8**, 349.
2 A. K. Bhagi, P. N. Kapoor, K. J. Klabunde and R. S. Mulukutla, *Dekker Encyclopedia of Nanoscience and Nanotechnology*, ed. J. A. Schwarz and C. I. Contescu, CRC Press, USA, 2004.
3 D. P. Nguyen, Q. T. Tran, X. S. Trinh, T. C. Hoang, H. N. Nguyen and H. H. Nguyen, *Adv. Nat. Sci.: Nanosci. Nanotechnol.*, 2012, **3**, 015017.
4 A. Demortière and C. Petit, *Langmuir*, 2007, **23**, 8575.
5 A. Khaleel, I. Shehadi and M. Al-Shamisi, *Colloids Surf., A*, 2010, **355**, 75.
6 M. Sorescu, L. Diamandescu, D. Tarabasanu-Mihaila, S. Krupa and M. Feder, *Hyperfine Interact.*, 2010, **196**, 359.
7 X. Liu, K. Shen, Y. Wang, Y. Wang, Y. Guo, Y. Guo, Z. Yong and G. Lu, *Catal. Commun.*, 2008, **9**, 2316.
8 D. P. Nguyen, X. S. Trinh, T. C. Hoang, N. D. Nguyen, V. T. Le, M. H. Nguyen, H. N. Nguyen and H. H. Nguyen, *J. Non-Cryst. Solids*, 2012, **358**, 537.
9 P. Reiss, M. Protière and L. Li, *Small*, 2009, **5**, 154.
10 B. P. Pichon, A. Demortiere, M. Pauly, K. Mougin, A. Derory and S. Begin-Colin, *J. Phys. Chem. C*, 2010, **114**, 9041.
11 A. Demortiére, P. Panissod, B. P. Pichon, G. Pourroy, D. Guillon, B. Donnio and S. Bégin-Colin, *Nanoscale*, 2011, **3**, 225.
12 G. Wirnsberger, K. Gatterer and P. Behrens, *J. Mater. Chem.*, 1998, **8**, 1509.
13 L. Lu, K. Hui-Zhong, M. Wenling, L. Huajie and W. Yuqiu, *J. Phys. Chem. B*, 2006, **110**, 15218.
14 M. Iijima, Y. Yonemochi, M. Tsukada and H. Kamiya, *J. Colloid Interface Sci.*, 2006, **298**, 202.
15 M. Mohapatra and S. Anand, *J. Eng. Sci. Technol. Rev.*, 2010, **2**, 127.
16 E. A. Deliyanni, L. Nalbandian and K. A. Matis, *J. Colloid Interface Sci.*, 2006, **302**, 458.
17 B. Che, *New Mesophase Morphologies Formed by Facial T-shaped Ternary Amphiphiles*, Martin Luther University of Halle-Wittenberg, Halle, Germany, 2004.
18 B. Rozic, M. Jagodic, S. Gyergyek, M. Drofenik, S. Kralj, G. Lahajnar, Z. Jaglicic and Z. Kutnjak, *Ferroelectrics*, 2011, **410**, 37.
19 A. Valor, E. Reguera, E. T. Garcia, S. Mendoza and F. S. Sinencio, *Thermochim. Acta*, 2002, **389**, 133.
20 W. W. Yu, J. C. Falkner, C. T. Yavuz and V. L. Colvin, *Chem. Commun.*, 2004, 2306.
21 J. E. Amonette and D. Rai, *Clays Clay Miner.*, 1990, **38**, 129.
22 K. Nakamoto, *Infrared and Raman Spectra of Inorganic and Coordination Compounds*, Wiley, John Wiley and Sons, Inc., USA, 1986.
23 A. L. Willis, N. J. Turro and S. O'Brien, *Chem. Mater.*, 2005, **17**, 5970.
24 A. L. Paterson, *Phys. Rev.*, 1939, **56**, 978.
25 J. M. Seddon, *Handbook of Liquid Crystals*, ed. D. Demus, J. Goodby, G. W. Gray, H. W. Spiess and V. Vill, Wiley-VCH, Weinheim, 1998, vol. 1, ch. 3.
26 A. Garcia-Marquez, A. Demortiere, B. Heinrich, D. Guillon, S. Begin-Colin and B. Donnio, *J. Mater. Chem.*, 2011, **21**, 8994.
27 V. A. Mallia, P. K. Vemula, G. John, A. Kumar and P. M. Ajayan, *Angew. Chem., Int. Ed.*, 2007, **46**, 1.
28 L. Cseh and G. H. Mehl, *J. Am. Chem. Soc.*, 2006, **128**, 13376.
29 M. Kaczmarek, O. Buchnev and I. Nandhakumar, *Appl. Phys. Lett.*, 2008, **92**, 103307.
30 A. J. Leadbetter, Structural classification of liquid crystals, in *Thermotropic Liquid Crystals*, Society of Chemical Industry, Gray, GW, UK, 1987.
31 D. K. Kim, Y. Zhang, W. Voit, K. V. Rao and M. Muhammed, *J. Magn. Magn. Mater.*, 2001, **225**, 30.
32 I. Chikazumi, *Physics of ferromagnetism*, Oxford Science Publications, Oxford University Press, USA, 1997.
33 T. Glowiak, M. Kubiak, T. Szymanska-Buzar and B. Jezowska-Trzebiatowska, *Acta Crystallogr., Sect. B: Struct. Crystallogr. Cryst. Chem.*, 1977, **33**, 3106.